

Short communication

# Photothermal effect of antimony-doped tin oxide nanocrystals on the photocatalysis

Shin-ichi Naya<sup>a</sup>, Yuya Shite<sup>b</sup>, Hiroaki Tada<sup>b,\*</sup><sup>a</sup> Environmental Research Laboratory, Kindai University, 3-4-1, Kowakae, Higashi-Osaka, Osaka 577-8502, Japan<sup>b</sup> Graduate School of Science and Engineering, Kindai University, 3-4-1, Kowakae, Higashi-Osaka, Osaka 577-8502, Japan

## ARTICLE INFO

## Keywords:

Plasmonic photocatalyst  
Photothermal effect  
Antimony-doped tin oxide  
Amine oxidation

## ABSTRACT

In the photocatalytic oxidation of amine by antimony-doped tin oxide nanocrystals under simulated sunlight ( $\lambda_{\text{ex}} > 300$  nm), significant enhancement of the activity and selectivity to aldehyde can be simultaneously achieved by the localized surface plasmon resonance-induced photothermal effect.

## 1. Introduction

Nanocrystals of heavily doped-metal oxide semiconductors such as antimony-doped tin oxide (SnO<sub>2</sub>: Sb) possess strong and broad absorption due to the surface plasmon resonance (LSPR) in the red, near-infrared (NIR) and IR region. Owing to the controllability of the LSPR in a wide wavelength range by varying doping level [1–3], the heavily doped-metal oxide semiconductor nanocrystals have found widespread interest because of the potential applications to a new class of smart windows [4,5], chemical and biosensing, telecommunications, advanced optics and photonics [6,7], and photocatalysis [8]. Recently, gold nanoparticle-based plasmonic photocatalysts have attracted much interest as a solar-to-chemical transformer [9–13], but the study on the metal oxide semiconductor nanocrystal-based plasmonic photocatalyst is still in its infancy [14,15]. While there are many reports on the photocatalytic activity of SnO<sub>2</sub> mainly for dye degradation [16–19], the photocatalysis of SnO<sub>2</sub>: Sb was only reported for polymerization of polyethyleneglycol diacrylate under irradiation of UV- or visible (Vis) light [20]. However, the LSPR-induced plasmonic effect of SnO<sub>2</sub>: Sb nanocrystals on the photocatalytic activity is unknown.

As the target reaction of this study, we selected amine oxidation, which is one of the important organic synthetic processes [21]. This study shows that the Sb-doping into SnO<sub>2</sub> enhances the photocatalytic activity and selectivity for the oxidation of amine to aldehyde due to the LSPR-induced photothermal effect.

## 2. Experimental

## 2.1. Catalyst preparation and characterization

Commercially available Sb-doped SnO<sub>2</sub> (SN-100P, Ishihara Sangyo Co., Sb doping amount = 11.6%, mean particle size = 9 nm, specific surface area = 70–80 m<sup>2</sup>g<sup>-1</sup>), TiO<sub>2</sub> (anatase, SSP-M, Sakai Chemical Industry co. mean particle size = 15 nm, specific surface area = 100 m<sup>2</sup>g<sup>-1</sup>) were used for the reaction. For transmission electron microscopy (TEM) characterization, samples were prepared by dropping of a suspension in ethanol onto a copper grid with carbon support collodion film (grid-pitch 150 μm, Okenshoji Co., Ltd., #10–1006). The TEM observations were examined by JEOL JEM-2100F at an applied voltage of 200 kV. X-ray diffraction (XRD) patterns were collected by means of a Rigaku SmartLab X-ray diffractometer operating at 40 kV and 100 mA. The scans were examined in the range from 20 to 90° (2θ) by the use of Cu Kα radiation ( $\lambda = 1.54059$  Å). The crystallite size (*D*) was calculated by the Scherrer eq. (1) from the full width at half maximum of the (110) diffraction peak.

$$D = \frac{K\lambda}{(\beta - B) \cos \theta} \quad (1)$$

where *K* is shape factor (0.9),  $\lambda$  is X-ray wavelength of Cu Kα (1.54059 Å),  $\beta$  is full width at half maximum, *B* is the broadening factor of the equipment (0.32),  $\theta$  is Bragg degree.

X-ray photoelectron spectroscopic (XPS) measurements were examined by means of a Kratos Axis Nova X-ray photoelectron spectrometer using a monochromated Al Kα X-ray source operated at 15 kV and 10 mA with C1s as the energy reference (284.6 eV). A Hitachi U-

\* Corresponding author.

E-mail address: [h-tada@apch.kidai.ac.jp](mailto:h-tada@apch.kidai.ac.jp) (H. Tada).<https://doi.org/10.1016/j.catcom.2020.106044>

Received 18 March 2020; Received in revised form 15 April 2020; Accepted 10 May 2020

Available online 16 May 2020

1566-7367/ © 2020 Published by Elsevier B.V.

4000 spectrometer with an integrating sphere were used for recording the diffuse reflectance UV–Vis–NIR spectra. The reflectance ( $R_\infty$ ) was recorded with respect to a reference of BaSO<sub>4</sub>, and the Kubelka-Munk function [ $F(R_\infty)$ ] expressing the relative absorption coefficient was calculated by the eq.  $F(R_\infty) = (1 - R_\infty)^2/2R_\infty$ .

## 2.2. Photocatalytic oxidation of amine

After the suspension of SnO<sub>2</sub>:Sb or TiO<sub>2</sub> (200 mg) in an acetonitrile solution of benzylamine (100 μM, 200 mL) had been stirred at room temperature (~20 °C), irradiation was started using a 300 W Xe lamp ( $\lambda > 300$  nm, HX-500, Wacom). The light intensity integrated from 320 to 400 nm ( $I_{320-400}$ ) was set to 2.6 mW cm<sup>-2</sup>. After removing particles by membrane filter, the amounts of products were quantified by high performance liquid chromatography (LC-6 CE, SPD-6 A, C-R8A (Shimadzu)) [measurement conditions: column = Shim-pack CLCDS (4.6 mm × 150 mm) (Shimadzu); mobile phase acetonitrile; flow rate = 1.0 mL min<sup>-1</sup>;  $\lambda = 280$  nm]. For evaluating the temperature dependence, the similar reactions were performed under the temperature controlled conditions from 15 to 42 °C by using double jacket with circulating water.

## 2.3. Photoelectrochemical measurement

Mesoporous (mp) nanocrystalline film of SnO<sub>2</sub>:Sb (12) was formed on fluorine-doped tin oxide (FTO, Aldrich, TEC 7). SnO<sub>2</sub>:Sb (12) was dispersed into a solution of Triton X-100 (0.1 mL), acetylacetone (1 drop), and polyethylene glycol 20,000 (0.2 g) in H<sub>2</sub>O (0.4 mL), and grinded to obtain the uniform paste. By doctor blade, the paste was coated on FTO with 60 μm thick, and the sample was calcined at 773 K for 1 h to obtain mp-SnO<sub>2</sub>:Sb/FTO electrode. Photocurrent response was examined by the standard three-electrochemical cell with the structure of mp-SnO<sub>2</sub>:Sb/FTO (working electrode) | 0.1 mM benzylamine + 0.1 M Bu<sub>4</sub>N·ClO<sub>4</sub> acetonitrile solution | Ag/AgCl (reference electrode) | glassy carbon (counter electrode). The working electrode was illuminated by monochromatic light using LED lamp. The incident photon-to-current efficiencies (IPCE) were calculated by Eq. 2.

$$\text{IPCE}[\%] = \frac{J_{\text{ph}}(E)N_{\text{A}}hc}{IF\lambda} \times 100 \quad (2)$$

where  $J_{\text{ph}}(E)$  is the photocurrent at an electrode potential of  $E$  (dark rest potential),  $N_{\text{A}}$  is Avogadro constant,  $h$  is Planck constant, and  $c$  is speed of light,  $I$  (W cm<sup>-2</sup>) is light intensity,  $F$  is Faraday constant.

## 2.4. Adsorption property

Adsorption amounts were obtained by exposing SnO<sub>2</sub>:Sb or TiO<sub>2</sub> (100 mg) to an acetonitrile solution of benzaldehyde or benzylamine (100 μM, 10 mL) at 25 °C or 45 °C for 3 h in the dark. After removing particles by membrane filter, the concentration of the remaining benzaldehyde or benzylamine was determined by HPLC.

## 3. Results and discussion

### 3.1. Catalysts characterization

SnO<sub>2</sub>: Sb particles with Sb-mole fraction ( $x_{\text{Sb}} / \text{mol}\% = \{\text{Sb} / (\text{Sn} + \text{Sb})\} \times 100$ ) = 0, 1.0, 11.6 (specific surface area = 70–80 m<sup>2</sup> g<sup>-1</sup>, SN-100P, Ishihara Sangyo), and for comparison, TiO<sub>2</sub> (anatase, SSP-M, Sakai Chemical Industry, mean particle size = 15 nm, specific surface area = 100 m<sup>2</sup>g<sup>-1</sup>) were used as the photocatalysts. The SnO<sub>2</sub> samples doped with  $x_{\text{Sb}} = 1.0\%$  and  $11.6\%$  are designated as SnO<sub>2</sub>: Sb (1) and SnO<sub>2</sub>: Sb (12), respectively. Fig. 1a shows transmission electron microscopy (TEM) image of SnO<sub>2</sub>: Sb (12). Almost sphere particles with an apparent size of ~9 nm are observed (Fig. S1). Fig. 1b shows high resolution (HR)-TEM image of the sample.

As shown by yellow lines, the lattice fringe has an interval of 2.65 Å, which is in agreement with the  $d$ -spacing of SnO<sub>2</sub>(101). Also, each particle in the TEM image is an aggregate consisting of several primary nanocrystals. Fig. 1c shows that the primary nanocrystal size distributes  $6.3 \pm 1.4$  nm. Fig. 1d shows X-ray diffraction patterns (XRD) for the samples. Every sample has peaks at  $2\theta = 26.88^\circ$ ,  $34.08^\circ$ ,  $38.10^\circ$ , and  $52.16^\circ$  assignable to the diffraction from the (110), (101), (200), and (211) crystal planes of SnO<sub>2</sub> with the rutile structure (ICDD No. 01-070-6995), respectively. No signal of antimony oxide phase is observed in the patterns of the Sb-doped samples. The broadening of the peaks is indicative of small crystalline domain sizes. The crystallite sizes of SnO<sub>2</sub>, SnO<sub>2</sub>: Sb (1), and SnO<sub>2</sub>: Sb (12) were calculated to be 6.3 nm, 6.2 nm, and 5.9 nm, respectively, by the Scherrer equation from the full-width at half maximum of the (110) diffraction peak. The value is in good agreement with the one determined by the HR-TEM observation.

Fig. 2a shows diffuse reflectance UV–Vis–NIR absorption spectra of SnO<sub>2</sub>: Sb with different doping amount, and the solar spectrum for comparison. In the spectrum for every sample, the absorption rises around 440 nm in spite that the band gap of stoichiometric SnO<sub>2</sub> is ~3.6 eV [22]. The absorption tail can result from the existence of oxygen vacancy [23]. Doping of Sb into SnO<sub>2</sub> nanocrystals causes the strong absorption in the red and NIR region. Also, the absorption edge of the interband transition is slightly blue-shifted by Sb-doping probably due to the Moss-Burstein effect raising the conduction band (cb) minimum [24]. X-ray photoelectron (XP) spectra were measured for SnO<sub>2</sub>: Sb with different doping level. In the Sn 3d-XP spectra for SnO<sub>2</sub>: Sb samples (Fig. S2), two signals due to the emission from the Sn 3d<sub>3/2</sub> and Sn 3d<sub>5/2</sub> orbitals of SnO<sub>2</sub> are observed regardless of  $x_{\text{Sb}}$  at the binding energies ( $E_{\text{B}}$ ) = 494.7 and 486.6 eV, respectively [25]. In the Sb 3d-XP spectra (Fig. 2b), the Sb 3d<sub>3/2</sub> signal is present at  $E_{\text{B}} = 539.8$  eV, which indicates that the Sb in SnO<sub>2</sub> mainly exists as Sb<sup>5+</sup> ion [26,27]. The signal of Sb 3d<sub>5/2</sub> at  $E_{\text{B}} \approx 531$  eV is overlapped with that of O 1s orbital. Thus, Sb-doping increases the density of free electrons, and the NIR-absorption in Fig. 2a is induced by the LSPR of which intensity increases with increasing  $x_{\text{Sb}}$  [1].

### 3.2. Photocatalytic amine oxidation

The photocatalytic activity of SnO<sub>2</sub>: Sb for benzylamine oxidation was studied. The photocatalytic activity was compared with that of TiO<sub>2</sub> as the representative semiconductor photocatalyst [28]. SnO<sub>2</sub>: Sb nanocrystals were dispersed into an acetonitrile solution of benzylamine, and stirred at room temperature in the dark for 0.5 h. Then, light was irradiated to the aerated suspension without cooling by using Xe lamp. Whereas no reaction occurred in the dark, photoirradiation of the solids (SnO<sub>2</sub>: Sb, SnO<sub>2</sub>, and TiO<sub>2</sub>) progresses the oxidation of benzylamine to yield benzaldehyde via the hydrolysis of the intermediate imine by residual water in the solvent (eq. 3) [29].



Fig. 3a shows time courses for benzaldehyde generation under irradiation of light with wavelength ( $\lambda_{\text{ex}}$ ) > 300 nm in the presence of SnO<sub>2</sub>: Sb, and SnO<sub>2</sub> and TiO<sub>2</sub> for comparison. TiO<sub>2</sub> shows high activity, but the maximum yield of benzaldehyde is lower than 75%. On the other hand, in the non-doped SnO<sub>2</sub> and SnO<sub>2</sub>: Sb (1) systems, the yield at irradiation time = 24 h is only ~60%. Strikingly, SnO<sub>2</sub>: Sb (12) exhibits much higher photocatalytic activity to generate benzaldehyde with a yield of ~90% at irradiation time = 24 h. Further, the yield continued to increase to reach 98% at irradiation time = 37 h. Irradiation of TiO<sub>2</sub> generates CO<sub>2</sub>, which is hardly generated in the SnO<sub>2</sub>: Sb (12) system (Fig. S3). Thus, the low yield of benzaldehyde in the TiO<sub>2</sub> system can be attributed to the overoxidation. To check the catalyst stability, 24 h-photocatalytic oxidation reaction of benzylamine was repeated 5 times using the catalyst particles retrieved from the suspension after each reaction (Fig. S4). No significant decay of the

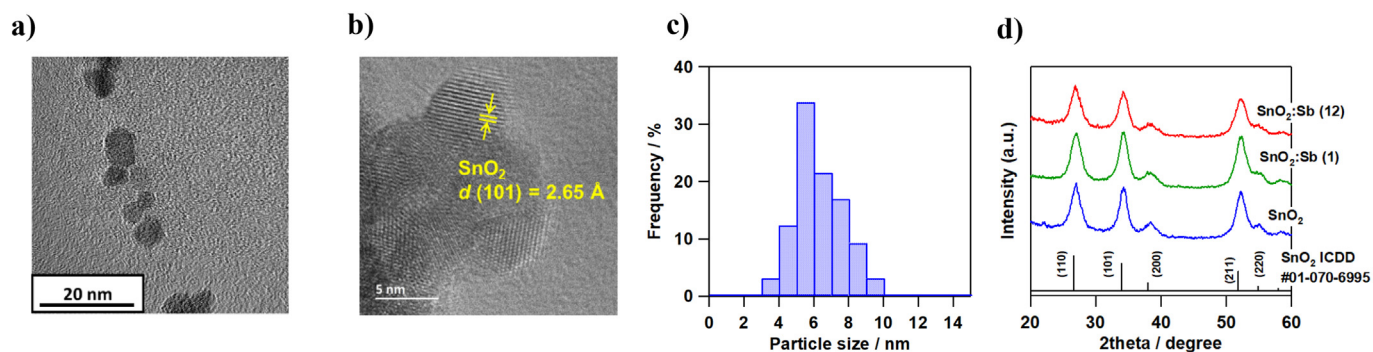


Fig. 1. TEM image (a) and HR-TEM (b) image of  $\text{SnO}_2\text{:Sb}$  (12). (c) Particle size distribution of  $\text{SnO}_2\text{:Sb}$  (12) determined by HR-TEM observation. (d) XRD patterns of  $\text{SnO}_2\text{:Sb}$  with different Sb-doping level.

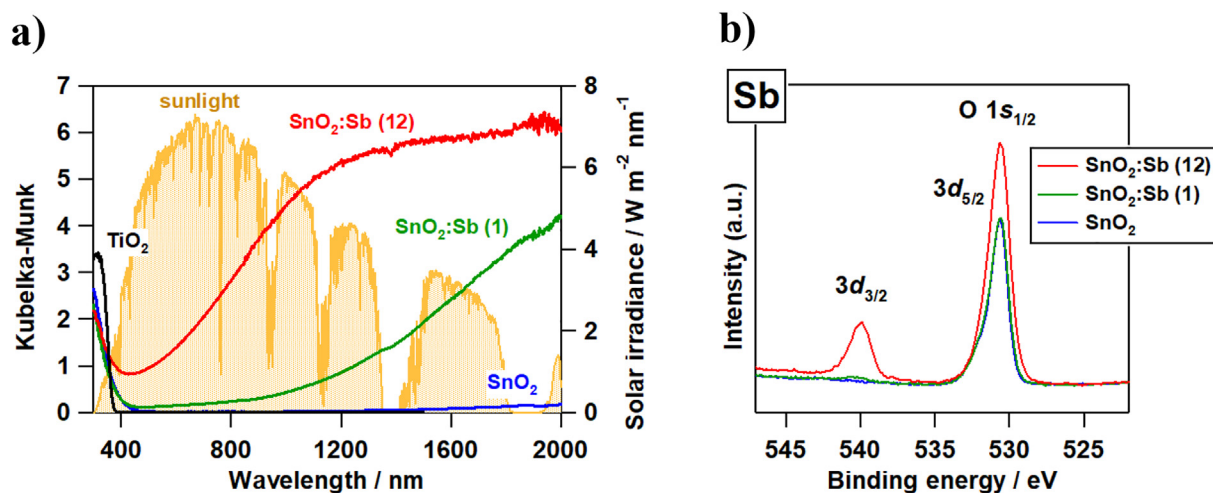


Fig. 2. (a) Diffuse reflectance UV-Vis-NIR absorption spectra of  $\text{SnO}_2\text{:Sb}$  with different doping amount ( $x_{\text{Sb}} = 0, 1.0, \text{ and } 11.6\%$ ), and solar irradiance spectrum for comparison. (b) Sb 3d-XP spectra of  $\text{SnO}_2\text{:Sb}$  with different doping amount.

photocatalytic activity is observed, indicating the high recyclability of the  $\text{SnO}_2\text{:Sb}$ .

### 3.3. Reaction mechanism

To gain insight into the reaction mechanism, the

photoelectrochemical (PEC) measurements were performed. A mesoporous film consisting of  $\text{SnO}_2\text{:Sb}$  (12) nanocrystals was formed on fluorine-doped  $\text{SnO}_2$  film (mp- $\text{SnO}_2\text{:Sb}$  (12)/FTO) electrode, and a three-electrode PEC cell was fabricated with the structure of mp- $\text{SnO}_2\text{:Sb}$  (12)/FTO (working electrode) | 0.1 mM benzylamine + 0.1 M  $\text{Bu}_4\text{NClO}_4$  acetonitrile solution | Ag/AgCl (reference electrode) | glassy

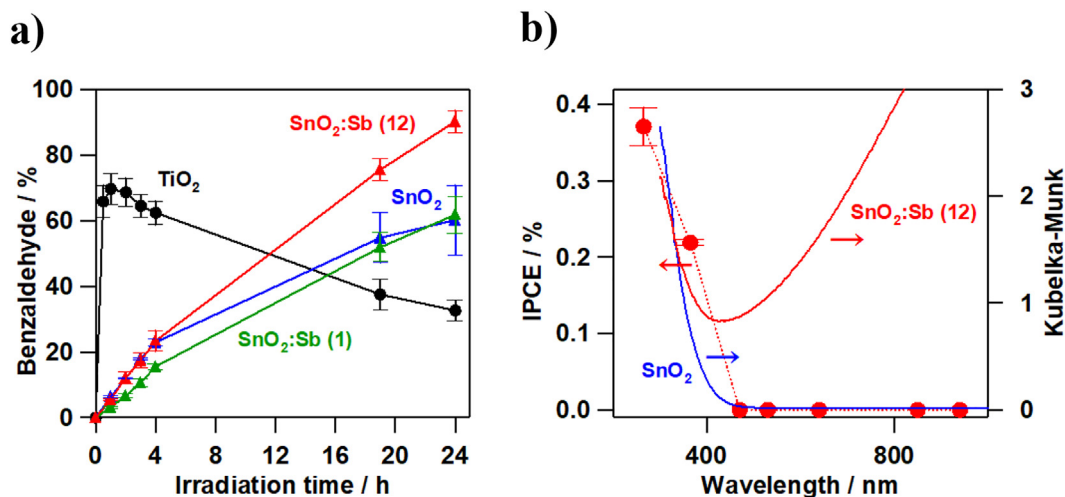


Fig. 3. (a) Time courses for benzaldehyde generation by photocatalytic oxidation of benzylamine by  $\text{SnO}_2\text{:Sb}$  ( $x_{\text{Sb}} = 0, 1.0, 11.6\%$ ) and  $\text{TiO}_2$  under photoillumination by Xe lamp without optical filter ( $\lambda_{\text{ex}} > 300 \text{ nm}$ , light intensity integrated from 320 nm to 400 nm =  $2.6 \text{ mW cm}^{-2}$ ). (b) IPCE action spectrum for benzylamine oxidation and the absorption spectrum for the catalyst is shown for comparison.

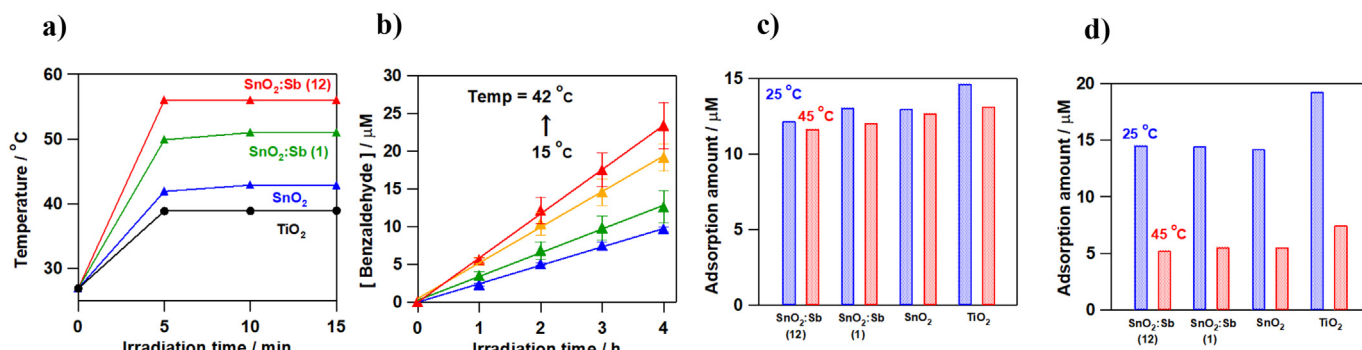


Fig. 4. (a) Time courses for the temperature of powder surface under photoirradiation. (b) Time courses for benzaldehyde generation under varying temperature with the photocatalytic oxidation of benzylamine. Adsorption property of benzylamine (c) and benzaldehyde (d) on the photocatalysts at 25 °C (blue) and 45 °C (red). (For interpretation of the references to colour in this figure legend, the reader is referred to the web version of this article.)

carbon (counter electrode). The currents were measured at the rest potential in the dark. First, stable photocurrent response was confirmed under irradiation by LED-lamp ( $\lambda_{\text{ex}} = 365 \text{ nm}$ , light intensity =  $3 \text{ mW cm}^{-2}$ ) (Fig. S5). Then, the photocurrents were measured under irradiation by LEDs with different emission wavelengths. Fig. 3b shows the action spectrum of incident photon-to-current efficiency (IPCE) for the mp-SnO<sub>2</sub>: Sb (12)/FTO electrode, and the absorption spectra of SnO<sub>2</sub> and SnO<sub>2</sub>: Sb (12) are also shown for comparison. The photocurrent is observed at  $\lambda_{\text{ex}} \leq 365 \text{ nm}$ , while the electrode shows no response at  $\lambda_{\text{ex}} \geq 470 \text{ nm}$ . Clearly, the SnO<sub>2</sub>: Sb (12)-photocatalyzed amine oxidation is caused by not the LSPR in the NIR region but the interband transition of SnO<sub>2</sub>.

The photocatalytic reactions were carried out without external cooling, and then, photoirradiation raised the temperature of the suspension. The temperature rise in each suspension system is more rapid than that in the solution system without particles (Fig. S6). Fig. 4a shows the temperature change of the powder without solution under the same irradiation conditions. In every system, the temperature increases to reach a constant value within 5 min. The increment in temperature is on the order of  $\text{TiO}_2 < \text{SnO}_2 < \text{SnO}_2: \text{Sb (1)} < \text{SnO}_2: \text{Sb (12)}$ , and the temperature of SnO<sub>2</sub>: Sb (12) exceeds 55 °C at the photostationary state. Clearly, the LSPR absorption of SnO<sub>2</sub>: Sb nanocrystals contributes to the increase in the temperature of the catalyst surface and the reaction suspension.

Next, the temperature effect on the rate of the amine oxidation was examined with the reaction temperature controlled by circulating constant-temperature water through the double jacket-type reaction cell. Fig. 4b shows time courses for the generation of benzaldehyde with the photocatalytic oxidation of benzylamine at different reaction temperatures. In every case, the concentration of benzaldehyde increases in proportion to irradiation time at  $< 4 \text{ h}$ , and the rate of reaction increases with increasing reaction temperature. The Arrhenius plot affords an apparent activation energy of  $25.0 \text{ kJ mol}^{-1}$  (Fig. S7), which is within the range reported so far for TiO<sub>2</sub> photocatalytic reaction systems ( $7.8\text{--}29.4 \text{ kJ mol}^{-1}$ ) [30–32]. Evidently, the temperature elevation by the NIR-absorption of SnO<sub>2</sub>: Sb (12) enhances the photocatalytic activity.

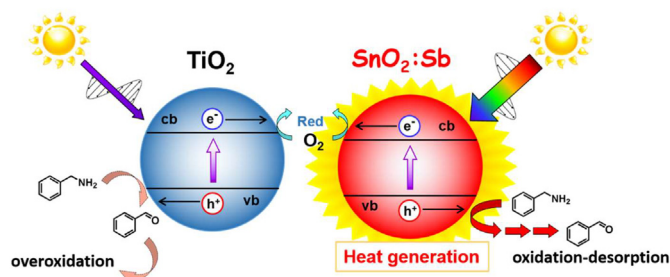
Further, the adsorption properties of benzylamine and benzaldehyde on the photocatalysts were examined at 25 °C and 45 °C. As shown in Fig. 4c, the temperature effect on the adsorption of benzylamine is small in every system. This would be probably because of the strong acid-base interaction between the solids and benzylamine. Thus, the supply of benzylamine (reactant) to the catalyst surface is hardly affected by the catalyst heating. Interestingly, Fig. 4d shows that the adsorption amount of benzaldehyde on each solid is drastically reduced with the increase in temperature. Also, Hu and Filler have recently reported that the desorption of indole and benzoic acid from indium tin oxide nanocrystals supporting NIR and mid-IR LSPR is enhanced by

irradiation with broadband IR light [33]. These results can be thermodynamically accounted for by the fact that the entropy of adsorption is usually negative. As such, the significant increase of temperature in the SnO<sub>2</sub>: Sb (12) system enhances the desorption of benzaldehyde (product) from the surface, which would restrict its overoxidation to increase the selectivity of the reaction. On the other hand, the overoxidation proceeds in the TiO<sub>2</sub> system because the photothermal product-desorption mechanism does not effectively work.

On the basis of these results, the action mechanism of the SnO<sub>2</sub>: Sb-photocatalyzed oxidation of benzylamine can be explained as follows (Scheme 1). Illumination of simulated sunlight ( $\lambda_{\text{ex}} > 300 \text{ nm}$ ) induces the band-gap excitation of SnO<sub>2</sub>: Sb. The holes generated in the valence band (vb) oxidize benzylamine to yield imine further undergoing hydrolysis to afford benzaldehyde (eq. 1). The electrons excited to the cb reduce the dissolved oxygen to complete the catalytic cycle. SnO<sub>2</sub>: Sb strongly absorbs the NIR-light under the irradiation conditions, raising the temperature near the photocatalyst surface to accelerate the oxidation of amine, simultaneously restrict the adsorption of aldehyde or its overoxidation. Consequently, a very high yield of  $\sim 98\%$  can be achieved at irradiation time = 37 h in the SnO<sub>2</sub>: Sb system. On the other hand, for the lack of the photothermal effect, the yield in the non-doped SnO<sub>2</sub> system remains  $\sim 60\%$  at irradiation time = 24 h, and the yield of the TiO<sub>2</sub> system is smaller than  $\sim 75\%$ .

#### 4. Conclusion

This study has shown that Sb-doped SnO<sub>2</sub> exhibits a high level of photocatalytic activity for the selective oxidation of amine to aldehyde due to the photothermal effect. We anticipate that Sb-doped SnO<sub>2</sub> nanocrystals can be widely used as a key component of the catalysts effectively utilizing the red, NIR, and IR in the sunlight for chemical transformations.



Scheme 1. Reaction mechanisms proposed for the photocatalytic oxidation of benzylamine to benzaldehyde by TiO<sub>2</sub> (left) and SnO<sub>2</sub>: Sb (right).

### Credit author statement

Shin-ichi Naya: Catalysts characterization, Photocatalytic reaction, and Adsorption properties, Yuya Shite: Catalysts characterization, Hiroaki Tada: Supervision the experimental work and data analysis.

### Declaration of Competing Interest

The authors declare that there is no conflict of interest.

### Acknowledgement

The authors acknowledge Ishihara Sangyo Co. for the gift of Sb doped-SnO<sub>2</sub> samples, and Y. Hamada for experimental support. This work was supported by JST Adaptable and Seamless Technology Transfer Program through Target-driven R&D, JSPS KAKENHI Grant-in-Aid for Scientific Research (C) no. 18 K05280 and 20 K05674, the Futaba Foundation, and Nippon Sheet Glass Foundation for Materials Science and Engineering.

### Appendix A. Supplementary data

Supplementary data to this article can be found online at <https://doi.org/10.1016/j.catcom.2020.106044>.

### References

- [1] J.M. Xu, L. Li, S. Wang, H.L. Ding, Y.X. Zhang, G.H. Li, *CrstEngComm* 15 (2013) 3296–3300.
- [2] G.V. Naik, V.M. Shalaev, A. Boltasseva, *Adv. Mater.* 25 (2013) 3264–3294.
- [3] S.D. Lounis, E.L. Runnerstrom, A. Llordés, D.J. Milliron, *J. Phys. Chem. Lett.* 5 (2014) 1564–1574.
- [4] G. Garcia, R. Buonsanti, E.L. Runnerstrom, R.J. Mendelsberg, A. Llordés, A. Anders, T.J. Richardson, D.J. Milliron, *Nano Lett.* 11 (2011) 4415–4420.
- [5] A. Llordés, G. Garcia, J. Gazquez, D.J. Milliron, *Nature* 500 (2013) 323–326.
- [6] A.L. Routzahn, S.L. White, L.K. Fong, P.K. Jain, *Isr. J. Chem.* 52 (2012) 983–991.
- [7] F. Scotognella, G. Valle, A.R. Srimath Kandada, M. Zavelani-Rossi, S. Longhi, G. Lanzani, F. Tassone, *Eur. Phys. J. B* 86 (2013) 154.
- [8] W. Liu, W. Zhang, M. Liu, P. Du, C. Dang, J. Liang, Y. Li, *Chin. Chem. Lett.* 30 (2019) 2177–2180.
- [9] K. Ueno, H. Misawa, *J. Photochem Photobiol C: Photochem Rev* 15 (2013) 31–52.
- [10] R. Jiang, B. Li, C. Fang, J. Wang, *Adv. Mater.* 26 (2014) 5274–5309.
- [11] L.C. Wang, D. Astruc, *Chem. Soc. Rev.* 43 (2014) 7188–7216.
- [12] X. Liu, L. Zhang, L. Yang, D. Ren, J. Wang, *Nat. Sci. Rev.* 4 (2017) 761–780.
- [13] H. Tada, *Dalton Trans.* 48 (2019) 6308–6313.
- [14] H. Cheng, T. Kamegawa, K. Mori, H. Yamashita, *Angew. Chem. Int. Ed.* 53 (2014) 2910–2914.
- [15] M. Sakamoto, T. Kawawaki, M. Kimura, T. Yoshinaga, J.J.M. Vequizo, H. Matsunaga, C.S.K. Ranasinghe, A. Yamakata, H. Matsuzaki, A. Furube, T. Teranishih, *Nat. Commun.* 10 (2019) 1879.
- [16] S. Wu, H. Cao, S. Yin, X. Liu, X. Zhang, *J. Phys. Chem. C* 113 (2009) 17893–17898.
- [17] H. Zhang, C. Hu, *Catal. Commun.* 14 (2011) 32–36.
- [18] S.P. Kim, M.Y. Choi, H.C. Choi, *Mater. Res. Bull.* 74 (2016) 85–89.
- [19] H. Xiao, F. Qu, A. Umar, X. Wu, *Mater. Res. Bull.* 74 (2016) 284–290.
- [20] J.C.M. Brokken-Zijp, O.L.J. van Asselen, W.E. Kleinjan, R. van de Belt, G. de With, *J. Nanotechnol.* (2011) 106254.
- [21] X. Lang, X. Chen, J. Zhao, *Chem. Soc. Rev.* 43 (2014) 473–486.
- [22] J. Zhang, W. Peng, Z. Chen, H. Chen, L. Han, *J. Mater. Chem. A* 1 (2013) 8453–8463.
- [23] T. Nütz, M. Haase, *J. Phys. Chem. B* 104 (2000) 8430–8437.
- [24] V. Kumar, A. Govind, R. Nagarajan, *Inorg. Chem.* 50 (2011) 5637–5345.
- [25] Y. Li, J. Liu, J. Liang, X. Yu, D. Li, *ACS Appl. Mater. Interfaces* 7 (2015) 6574–6583.
- [26] C. Terrier, J.P. Chatelon, J.A. Roger, R. Berjoan, C. Dubois, *J. Sol-Gel Sci, Technol.* 10 (1997) 75–81.
- [27] Y. Li, J. Liu, J. Liang, X. Yu, D. Li, *ACS Appl. Mater. Interfaces* 7 (2015) 6574–6583.
- [28] D. Friedmann, A. Hakki, H. Kim, W. Choi, D. Bahnmann, *Green Chem.* 18 (2016) 5391–5411.
- [29] Y. Sato, S. Naya, H. Tada, *APL Mater.* 3 (2015) 104502–1–7.
- [30] H. Tada, F. Suzuki, S. Yoneda, S. Ito, H. Kobayashi, *Phys. Chem. Chem. Phys.* 3 (2001) 1376–1382.
- [31] Ö.E. Kartal, E. Erol, H. Oğuz, *Chem. Eng. Technol.* 24 (2001) 645–649.
- [32] A.E.H. Machado, J.A. de Miranda, R.F. de Freitas, E.T.F.M. Duarte, L.F. Fer-reira, Y.D.T. Albuquerque, R. Ruggiero, C. Sallter, L. Oliveira, *J. Photochem. Photobiol. A: Chem.* 155 (2003) 231–241.
- [33] W. Hu, M.A. Filler, *J. Vacuum Sci, Technol.* 36 (2018) 061401–1–6.